Monthly Notices of the ROYAL ASTRONOMICAL SOCIETY
MNRAS **519,** 26–33 (2023) https://doi.org/10.1093/mnras/stac2929

Light pollution indicators for all the major astronomical observatories

Fabio Falchi [1,2]★ Felipe Ramos,[3] Salvador Bará,[4] Pedro Sanhueza,[5] Marcelo Jaque Arancibia,[6] Guillermo Damke[7] and Pierantonio Cinzano[2]

[1]*Departamento de Física Aplicada, Universidade de Santiago de Compostela, Santiago de Compostela, 15782 Galicia, Spain*
[2]*ISTIL Istituto di Scienza e Tecnologia dell'Inquinamento Luminoso – Light Pollution Science and Technology Institute, I-36016 Thiene, Italy*
[3]*Instituto de Investigación Multidisciplinar en Ciencia y Tecnología, Universidad de La Serena, 1720170 La Serena, Chile*
[4]*Independent scholar, Santiago de Compostela, Galicia, Spain*
[5]*OPCC Oficina de Protección de la Calidad del Cielo del Norte de Chile, 1700000 La Serena, Chile*
[6]*Departamento de Física y Astronomía, Universidad de La Serena, 1720236 La Serena, Chile*
[7]*Cerro Tololo Inter-American Observatory/NSF's NOIRLab, 1700000 La Serena, Chile*

Accepted 2022 October 3. in original form 2022 September 10

ABSTRACT

Light pollution at astronomical observatories is one of the main factors to be taken into account to preserve their scientific productivity and their useful lifetime. Using the Garstang–Cinzano model applied to the Visible Infrared Imaging Radiometer Suite (VIIRS) 2021 satellite radiance data, we have compared 28 sites, all hosting telescopes with apertures larger than 3 m, plus some additional selected sites. We computed and analysed five indicators of light pollution: radiance at zenith; averaged at 60° zenith distance; averaged over all the sky; averaged in the first 10° above the horizon; and horizontal irradiance. We found large variations of the values of the indicators, with a factor greater than 600 for the zenith artificial radiance between the least and most polluted major observatories. The results show that two-thirds of all large observatories have already surpassed the critical 10 per cent increase in radiance over the assumed natural levels. The results presented and the method described here can help to plan countermeasures in order to lower the impact of light pollution on observatories. These same methods can be also used to protect the night environment from the impact of artificial light (e.g. on biodiversity, on animal behaviour and physiology, on human health).

Key words: atmospheric effects – light pollution – site testing.

1 INTRODUCTION

Light pollution, the alteration of the natural lighting levels in the night environment due to human activities, is rapidly increasing globally (Kyba et al. 2017; Sánchez de Miguel et al. 2021). These human activities include all the artificial light at night (ALAN) produced outdoors or that escapes outdoors coming from indoors (e.g. windows, shops, greenhouses) and the light of the Sun reflected into the night hemisphere by orbiting satellites and space debris (Kocifaj et al. 2021). The state of light pollution around the world has been globally described by two world atlases of artificial sky brightness (Cinzano et al. 2001a; Falchi et al. 2016a). These atlases quantify the quality of the night sky using the radiance at zenith.

This study is a comprehensive comparison of all the main professional astronomical observatories around the world, evaluating, beside the zenith radiance, four other light pollution indicators, each with its specificity in describing the night sky quality (Falchi & Bará 2021). To compute the indicators, we used the Garstang–Cinzano light propagation model (Garstang 1986; Garstang 1989; Cinzano & Elvidge 2004) applied to the radiance-calibrated *Suomi National Polar-orbiting Partnership* (*NPP*) satellite's Visible Infrared Imaging Radiometer Suite (VIIRS) Annual VNL V2 median-masked data for the year 2021 (Elvidge et al., 2021). We take into account the screening due to the Earth's curvature and the altitudes above sea level of the observatories and sources, as provided by the Global Multi-resolution Terrain Elevation Data 2010 (GMTED2010; Danielson and Gesch 2011), and we sum the contribution of all sources in a radius of 500 km from the observatory's site. The input rasters have pixel dimensions of 15 × 15 arcsec^2, corresponding to 463 × 463 m^2 square pixel size at the equator and progressively narrowing in the east–west direction with increasing latitude. For calculations, we resampled the rasters to obtain a uniform 400 × 400 m^2 pixel size for any latitude. In order to automate image cutting of VIIRS and GMTED data, pixel resize, raster alignment, generation of point spread function (PSF) rasters and final calculations, we used a Python code based on the GRASS GIS API.

The actual sky quality at observatories can vary, for different reasons, when compared with the quality computed in this work. For example, regarding the main sources of artificial light, cloud cover will darken the sky or, conversely, a particularly clean atmosphere over a distant city might increase the light pollution coming from that light source. As said, the model takes into account the screening due to the Earth's curvature, while it neglects the screening from mountains. This approximation usually introduces very small differences in the values of the indicators. For example, the zenith radiance at Roques de Los Muchachos is lowered by less than 20 per cent and

★ E-mail: falchi@lightpollution.it

© 2022 The Author(s)
Published by Oxford University Press on behalf of Royal Astronomical Society

Downloaded from https://academic.oup.com/mnras/article/519/1/26/6936422 by guest on 09 January 2025

Cerro Tololo is practically unaffected by the screening introduced by the orography of the region (see figs 7 and 8 in Cinzano et al. 2001b).

To improve the models and to monitor the sky quality over time, it would be extremely helpful for each observatory to continuously collect and distribute, in open-access form, all-sky radiance and extinction data, in different bands. This will also assist in better planning countermeasures to protect the long-term productivity of telescopes.

2 MATERIALS AND METHODS

The indicators chosen for this study, all evaluated in the astronomical Johnson *V* band (550 nm effective wavelength mid-point), are the zenith radiance, the average all-sky radiance, the average radiance at 60° zenith distance, the average radiance in the first 10° above the horizon and the horizontal irradiance.

These indicators were computed using the Garstang–Cinzano light propagation model using a clarity parameter $K' = 1$ (see Cinzano et al. 2000; Cinzano & Elvidge 2004), which describes a US62 standard atmosphere with an inverse scale altitude $c = 0.104$ km^{-1} and a molecular density at sea level $N_{m,0} = 2.55 \times 10^{19}$ cm^{-3}. This model of the atmosphere proved to be adequate for describing the sky above the observing sites, despite the wide range of locations around the world, as shown by the comparison between the extinction factors calculated with the model and the average or median extinction factors measured in photometric nights at the observatories (for which data were found; see Table 2). The greatest difference between the extinction factor used in our computation and the reported measured extinction factor at an observatory is less than 0.03 mag, and in most cases it is less than 0.01 mag.

Our work takes advantage of the use of analytical PSFs obtained by fitting the discrete value PSFs computed, for each indicator, by the Fortran code developed by Cinzano, and updated and adapted for the purpose by Falchi. The code gave the radiance in 10 115 directions in a half-hemisphere uniformly distributed in a Zenith Equal Area projection (Calabretta & Greisen 2002). Thus, each elemental area in the computed map corresponds to a fixed same solid angle in the sky of 3.1×10^{-4} sr, which corresponds to about 1 deg^2. The computation of the radiances in these directions in the sky hemisphere was repeated for distances from 0.12 km to 527 km, in incremental steps with a 1.2× multiplication factor. This was all repeated for nine altitudes above the sea level of the observing sites from 0 m to 5600 m (0, 500, 1000, 1500, 2000, 2500, 3000, 4000, 5600 m) and for 11 altitudes of the light sources (0, 250, 500, 750, 1000, 1250, 1500, 2000, 2500, 3000, 4000 m), with all the combinations where the sources are at an equal or lower altitude of the observing site. The computation was repeated for three different shapes of the intensity of the light source as a function of the emission angle (i.e. the upward emission function, UEF). For each combination of source and site altitude, a linear combination of the three PSFs was made in order to obtain the PSFs for the UEF that was retrieved from the New World Atlas of Artificial Sky Brightness (hereafter NWA; Falchi et al. 2016a). This finally generated 325 PSFs that were used to obtain the analytical best-fitting functions. An additional 95 PSFs were generated for different site altitudes in order to check independently the good fit of the analytical functions.

The analytical functions give, for each indicator, the LOG10 value of the PSF as a function of three variables: the LOG10 of the horizontal distance between observer and source, the observer's altitude, and the source's altitude. These functions were found by running NDCURVEMASTER, an *n*-dimensional non-linear curve and surface fitting program[1] and allowing it to use polynomials, exponentials, power functions, logarithms and their combinations. The search for a best-fitting formula was stopped after a root mean square error (RMSE) of 0.06 or less was obtained along with less than 15 terms in the equations.

2.1. Analytical functions describing the PSFs

The analytical functions used in this work are the following. The independent variables are the altitude above sea level of the observatory's site h_{obs}, the altitude of the sources of light h_s (which should be lower than or equal to h_{obs}) and the distance D from the observatory's site, all expressed in km.

If the following PSFs are used with VIIRS radiance data in nW cm^{-2} sr^{-1} and pixel area in km^2, to obtain the results of the radiances in W m^{-2} sr^{-1} and the irradiance in W m^{-2}, an additional term Cf = −7,86 should be added in the following equations. This term is the log10 of the calibration factor described in section 2.2.

2.1.1. Zenith radiance

The zenith radiance indicator gives the radiance in the direction of zenith. It can be relatively forgiving of the polluted status of the night sky, especially in areas with low light pollution, with the zenith usually being the less contaminated direction of the night sky.

The zenith sky radiance (ZSB) indicator PSF has 12 terms, an RMSE of 0.0491, and an R^2 of 0.99948. Its analytical formula is

$$\begin{aligned}\log_{10} PSF_ZSB = {} & a_0 + a_1 h_{obs}^{0.34} + a_2 2^{\log D} + a_3 h_{obs}^{-1.5} + a_4 h_{obs}^{0.49} \\ & + a_5 (\log D)^4 \left(\frac{1}{2}\right)^{h_s} + a_6 h_{obs}^{-1.15} h_s^{1.5} + a_7 (\log D)^{11} \\ & + a_8 (\log D)^4 + a_9 \left(\frac{1}{6}\right)^{\log D} + a_{10} (\ln h_{obs})^8 h_s^{0.76} \\ & + a_{11} (\log D)^2. \end{aligned} \quad (1)$$

Here, $a_0 = 1.57971$, $a_1 = 0.266809$, $a_2 = -1.88908$, $a_3 = -0.150676$, $a_4 = -0.793737$, $a_5 = -0.0282754$, $a_6 = 0.440433$, $a_7 = -0.0000189817$, $a_8 = 0.0657736$, $a_9 = 0.0430336$, $a_{10} = -0.000041948$, and $a_{11} = 0.111841$.

2.1.2. Average all-sky radiance

The average radiance in the whole night-sky hemisphere is obtained by averaging the values of the radiance in a sufficiently dense number of directions in the sky, 20 149 in our computation. The directions are chosen so that each corresponds to an equal area of the sky, approximately 1 deg^2. Arguably, this is the single indicator that describes best the overall situation of the night-sky hemisphere.

The PSF of the indicator of the average radiance in the whole night-sky hemisphere has 11 terms, an RMSE of 0.0539, and an R^2 of 0.99886. Its analytical formula is

$$\begin{aligned}\log_{10} PSF_AllSkyAvBri = {} & a_0 + a_1 h_{obs}^{0.47} + a_2 \left(\frac{1}{2}\right)^{h_s} + a_3 2^{\log D} \\ & + a_4 h_{obs}^{-7} h_s^6 + a_5 h_{obs}^{0.42} \log D + a_6 h_s^{0.01} (\log D)^3 \\ & + a_7 h_{obs}^{-2.7} h_s^{2.95} \left(\frac{1}{3}\right)^{\log D} + a_8 (\log D)^{16} + a_9 h_s \log D \\ & + a_{10} \left(\frac{1}{2}\right)^{h_{obs}} \left(\frac{1}{2}\right)^{\log D}. \end{aligned} \quad (2)$$

[1] www.ndcurvemaster.com

Downloaded from https://academic.oup.com/mnras/article/519/1/26/6936422 by guest on 09 January 2025

Table 1. All the studied sites's coordinates, altitudes and light pollution indicators.

Site	Type	Longitude (deg)	Latitude (deg)	Altitude (m)	Zenith radiance (W m^{-2} sr^{-1})	Average radiance (all sky) (W m^{-2} sr^{-1})	Average radiance at 30° (W m^{-2} sr^{-1})	Average radiance below 10° (W m^{-2} sr^{-1})	Horizontal irradiance (W m^{-2})
Maui A.F. Optical Station	Observatory	−156.25700	20.70820	3036	1.17E−08	4.19E−08	2.84E−08	1.64E−07	8.35E−08
Mauna Kea	Observatory	−155.47253	19.82464	4160	2.33E−09	1.54E−08	7.98E−09	6.22E−08	2.48E−08
Mauna Kea (NO volcano)	Observatory	−154.47253	20.82464	4160	1.73E−09	9.25E−09	4.96E−09	4.40E−08	1.56E−08
Lick	Observatory	−121.63732	37.34285	1260	3.06E−07	1.29E−06	8.93E−07	3.88E−06	2.39E−06
Palomar	Observatory	−116.86500	33.35660	1712	1.34E−07	7.99E−07	4.65E−07	2.70E−06	1.30E−06
San Pedro Martir	Observatory	−115.46370	31.04410	2795	2.14E−09	1.66E−08	6.44E−09	1.31E−07	2.10E−08
Kitt Peak	Observatory	−111.59991	31.96394	2050	1.34E−08	1.33E−07	6.86E−08	4.29E−07	2.00E−07
Lowell Discovery Tel.	Observatory	−111.42200	34.74460	2353	5.83E−09	7.51E−08	3.55E−08	2.49E−07	1.06E−07
Whipple	Observatory	−110.88507	31.68892	2580	2.83E−08	2.59E−07	1.44E−07	8.35E−07	4.03E−07
Mount Graham	Observatory	−109.88920	32.70128	3191	1.36E−08	1.10E−07	5.91E−08	3.44E−07	1.72E−07
Starfire Optical Range	Observatory	−106.46349	34.96415	1872	2.27E−07	2.03E−06	1.26E−06	6.62E−06	3.28E−06
Apache Point	Observatory	−105.82023	32.78027	2790	1.92E−08	1.73E−07	9.91E−08	5.30E−07	2.80E−07
McDonald	Observatory	−104.01472	30.68145	2026	4.16E−09	5.57E−08	2.77E−08	1.82E−07	8.39E−08
Cerro Tololo	Observatory	−70.80653	−30.16966	2205	1.37E−08	8.01E−08	4.77E−08	2.63E−07	1.32E−07
Pachon	Observatory	−70.74235	−30.24352	2707	9.82E−09	6.10E−08	3.39E−08	2.06E−07	9.77E−08
La Silla	Observatory	−70.73248	−29.25995	2360	2.88E−09	2.35E−08	1.22E−08	8.26E−08	3.53E−08
Las Campanas (Magellan)	Observatory	−70.69239	−29.01429	2380	3.79E−09	2.89E−08	1.63E−08	9.56E−08	4.55E−08
Las Campanas (GMT)	Observatory	−70.68216	−29.04877	2516	3.34E−09	2.66E−08	1.46E−08	8.97E−08	4.12E−08
Paranal	Observatory	−70.40417	−24.62722	2635	4.90E−10	5.96E−09	2.73E−09	2.81E−08	8.71E−09
Armazones (NO lodge)	Observatory	−70.19160	−24.59100	3046	5.43E−10	8.05E−09	3.62E−09	3.67E−08	1.15E−08
Armazones	Observatory	−70.19160	−24.59100	3046	1.75E−09	1.17E−08	6.60E−09	4.29E−08	2.09E−08
Tokyo Atacama	Observatory	−67.74225	−22.98629	5640	5.59E−10	1.28E−08	5.87E−09	4.26E−08	1.85E−08
Roque de los Muchachos	Observatory	−17.88642	28.75829	2344	1.39E−08	4.67E−08	3.46E−08	1.49E−07	9.71E−08
Calar Alto	Observatory	−2.54685	37.22079	2160	4.21E−08	2.56E−07	1.48E−07	9.37E−07	4.18E−07
South African AO	Observatory	20.81080	−32.37597	1760	6.00E−10	5.31E−09	2.93E−09	1.85E−08	8.01E−09
SAO BTA-6	Observatory	41.44045	43.64683	2070	1.02E−08	7.87E−08	4.42E−08	2.76E−07	1.25E−07
ARIES Devasthal Obs.	Observatory	79.68464	29.36110	2420	3.65E−08	2.31E−07	1.34E−07	7.02E−07	3.79E−07
SST (Nav. Comm. Holt)	Observatory	114.09 011	−21.89574	59	2.03E−08	9.19E−08	7.47E−08	3.71E−07	1.54E−07
Beijing Astron. Obs.	Observatory	117.57586	40.39576	880	1.03E−07	5.16E−07	3.43E−07	1.49E−06	9.32E−07
Australian Astron. Obs.	Observatory	149.06700	−31.27560	1130	6.21E−10	4.19E−09	2.49E−09	1.18E−08	6.80E−09
Macon	Potential site	−67.25955	−24.46540	5500	2.81E−10	9.73E−09	3.89E−09	3.54E−08	1.24E−08
Muztagh	Potential site	74.89700	38.33200	4526	1.28E−09	1.44E−08	6.98E−09	4.33E−08	2.19E−08
Ali	Potential site	80.04600	32.30800	5100	2.18E−09	4.14E−08	1.81E−08	1.08E−07	5.30E−08
NAOC Saishiteng Mt	Potential site	93.89584	38.60655	4215	9.89E−11	3.37E−09	1.60E−09	1.20E−08	4.89E−09
Daocheng	Potential site	100.10900	29.10900	4750	1.56E−09	2.32E−08	1.15E−08	6.37E−08	3.37E−08
Wilson	Historic/control obs.	−118.05718	34.22591	1742	1.30E−06	5.39E−06	3.68E−06	1.56E−05	1.00E−05
Lowell Mars Hill	Historic/control obs.	−111.66464	35.20292	2212	3.25E−07	1.45E−06	1.04E−06	3.40E−06	3.10E−06
Lowell Anderson Mesa	Historic/control obs.	−111.53677	35.09707	2204	1.93E−08	2.15E−07	1.22E−07	6.84E−07	3.27E−07
Chapultepec	Historic/control obs.	−99.18185	19.42047	2282	4.92E−06	3.29E−05	2.10E−05	8.91E−05	5.91E−05
Mont Megantic	Historic/control obs.	−71.15277	45.45579	1100	1.62E−08	9.88E−08	5.84E−08	2.60E−07	1.61E−07
Pic du Midi	Historic/control obs.	0.14162	42.93674	2877	3.19E−08	2.00E−07	1.09E−07	6.64E−07	3.17E−07
Brera-Merate	Historic/control obs.	9.42915	45.70592	332	2.75E−06	1.21E−05	9.19E−06	3.95E−05	2.32E−05
Asiago	Historic/control obs.	11.56901	45.84857	1360	3.91E−07	1.77E−06	1.22E−06	5.35E−06	3.31E−06
Pulkovo	Historic/control obs.	30.32615	59.77182	80	5.67E−06	2.28E−05	1.83E−05	7.87E−05	3.92E−05
New Mexico Skies	Amateur observatory	−105.52923	32.90331	2224	9.93E−09	9.99E−08	5.50E−08	3.13E−07	1.62E−07
El Sauce, Chile	Amateur observatory	−70.76488	−30.47062	1540	7.69E−09	5.30E−08	3.14E−08	1.65E−07	8.54E−08
El Pangue, Chile	Amateur observatory	−70.69424	−30.14302	1478	1.57E−08	8.83E−08	5.84E−08	2.71E−07	1.55E−07
Celestial Exploration, Chile	Amateur observatory	−68.17948	−22.95280	2397	2.33E−08	1.53E−07	9.82E−08	3.98E−07	2.84E−07
Athos Centro Astronomico, La Palma	Amateur observatory	−17.95875	28.77770	875	2.39E−08	8.86E−08	6.33E−08	2.42E−07	1.79E−07
AstroFarm La Palma	Amateur observatory	−17.93469	28.78587	1155	1.17E−08	4.91E−08	3.73E−08	1.63E−07	9.89E−08
Tivoli Astro Farm, Namibia	Amateur observatory	18.01585	−23.46130	1340	1.25E−10	2.28E−09	1.14E−09	6.73E−09	3.43E−09
Baja California	Control site	−114.1518	31.5057	23	2.62E−09	5.96E−09	7.15E−09	2.57E−08	1.60E−08
Sierra Estrella	Control site	−112.2796	33.2738	1325	5.25E−07	2.81E−06	1.93E−06	8.11E−06	5.00E−06
40 km North Mexico City	Control site	−99.2949	19.7616	2844	5.50E−07	6.10E−06	3.44E−06	1.74E−05	9.48E−06
San Benedetto Po	Control site	10.9196	45.0511	20	9.96E−07	1.34E−06	3.71E−06	1.46E−05	7.09E−06
Baltic Sea (Bothnia Bay)	Control site	22.6992	64.6519	0	1.09E−09	2.70E−09	6.41E−10	1.16E−08	9.51E−09

Here, $a_0 = 2.45186$, $a_1 = -0.949292$, $a_2 = -0.232895$, $a_3 = -1.85463$, $a_4 = -0.0432241$, $a_5 = 0.631389$, $a_6 = 0.0910021$, $a_7 = 0.463856$, $a_8 = -1.68834\text{E}{-8}$, $a_9 = 0.00308806$, and $a_{10} = 0.00645667$.

2.1.3. Average radiance 30° above the horizon (computed with zenith distance between 59°.5 to 60°.5)

The indicator that describes the average radiance at 60° zenith distance (i.e. 30° above the horizon) is very apt to indicate the suitability of the night sky for astronomical research. This because

Downloaded from https://academic.oup.com/mnras/article/519/1/26/6936422 by guest on 09 January 2025

Table 2. List of observatories where extinction data were found (last column), along with altitude of the site, the optical depth and the extinction in magnitudes corresponding, for each altitude, to $K' = 1$ at sea level.

Site name	Altitude (m)	Optical depth τ	Extinction Kv for $K' = 1$ (mag)	Measured extinction Kv (mag)
Mauna Kea Observatories	4160	0.083	0.090	0.103[a]
La Silla Observatory	2360	0.124	0.134	0.13[b]
Roque de los Muchachos Obs.	2344	0.124	0.135	0.13[c]
Paranal Observatory	2635	0.115	0.125	0.13[d]
Apache Point Obs.	2790	0.111	0.120	0.14[e]
Palomar Observatory	1712	0.151	0.164	0.158[f]
Lick Observatory	1260	0.177	0.192	0.183[g]
Beijing Astronomical Obs.	880	0.206	0.223	0.228[h]
San Pedro Martir	2795	0.110	0.120	0.13[i]
Calar Alto Observatory	2160	0.131	0.142	0.15[j]
Devasthal Observatory	2450	0.121	0.131	0.16[k]
Siding Spring	1130	0.186	0.202	0.18[k]
McDonald Observatory	2026	0.137	0.148	0.16[l]
Cerro Tololo	2210	0.129	0.140	0.14[m]

[a]From figure 12 of Buton et al. (2013).
[b]From table 4 of Hogg et al. (2001).
[c]From table 2 of García-Gil, Muñoz-Tuñón & Varela (2010).
[d]From figure 2 of Pata et al. (2011).
[e]From Hogg et al. (2001).
[f]From table 2 of Hayes & Latham (1975).
[g]From https://mthamilton.ucolick.org/techdocs/standards/lick_mean_extinct.html.
[h]Mean of values in table 6 of Bai et al. (2018).
[i]Median value from Tapia, Cruz-González & Avila (2007).
[j]Winter value, as summer values extremely variable; see figure 2 of Sánchez et al. (2007).
[k]From figure 1 of Mohan et al. (1999).
[l]From figure 1 (maximum of the fit) of Angione & de Vaucouleurs (1986).
[m]From table 1 of Gutierrez-Moreno, Cortes & Moreno (1982).

the great part of astronomical research is carried out pointing the telescopes at no less than 30° above the horizon, to limit somehow the negative effects of our atmosphere, such as the absorption of light coming from studied celestial objects and the degradation due to turbulence (astronomical seeing).

The PSF of the indicator of the average radiance at 30° altitude (average of the radiance from 59.°5 to 60.°5 zenith distance) has 14 terms, an RMSE of 0.0576, and an R^2 of 0.99918. Its analytical formula is

$$\begin{aligned}\log_{10} PSF_AvBri30 = {} & a_0 + a_1 h_{\rm obs}^{0.46} + a_2 \left(\frac{1}{4}\right)^{h_{\rm s}} + a_3 2^{\log D} \\ & + a_4 h_{\rm obs}^{-1.55} h_{\rm s}^2 + a_5 h_{\rm obs}^{0.36} \log D + a_6 h_{\rm s}^{0.78} (\log D)^3 \\ & + a_7 h_{\rm obs}^{-1.7} h_{\rm s}^{2.05} \left(\frac{1}{2}\right)^{\log D} + a_6 h_{\rm s}^{0.78} (\log D)^3 \\ & + a_7 h_{\rm obs}^{-1.7} h_{\rm s}^{2.05} \left(\frac{1}{2}\right)^{\log D} + a_8 (\log D)^{16} + a_9 h_{\rm obs}^{5.25} h_{\rm s}^6 + a_{10} e^{5 h_{\rm obs}} \\ & + a_{11} e^{-3 h_{\rm obs}} h_{\rm s} + a_{12} (\ln h_{\rm obs})^3 + a_{13} (\log D)^7. \end{aligned} \quad (3)$$

Here, $a_0 = 1.88212$, $a_1 = -0.839652$, $a_2 = -0.0866602$, $a_3 = -1.65433$, $a_4 = -0.239984$, $a_5 = 0.545403$, $a_6 = 0.0239902$, $a_7 = 0.698956$, $a_8 = -7.78489\text{E}{-8}$, $a_9 = -1.1881\text{E}{-9}$, $a_{10} = 1.25288\text{E}{-14}$, $a_{11} = -0.41677$, $a_{12} = 0.00007752$, and $a_{13} = 0.0006342$.

2.1.4. *Average radiance 0° to 10° above the horizon*

The average radiance in the first 10° above the horizon has a lower direct impact on astronomical research even if it is of greater importance for the amateur astronomer and the common citizen, who want to appreciate a wilderness experience during the night. This is because the first degrees above the horizon are where the impact of very far light pollution sources is first revealed, ruining the landscape even at hundreds of kilometres away from big cities; for example, Las Vegas and Phoenix glows can be seen from the Grand Canyon National Park, and Honolulu can be seen from the Mauna Kea summit. Moreover, the impact in the first degrees above the horizon is a preliminary warning that the sky is beginning to be polluted and that immediate action is necessary to preserve its quality for astronomical research.

The PSF of the indicator of the average radiance in the first 10° above the horizon has 15 terms, an RMSE of 0.0593, and an R^2 of 0.99878. Its analytical formula is

$$\begin{aligned}\log_{10} PSF_AvBriBelow10 = {} & a_0 + a_1 h_{\rm obs}^{0.41} + a_2 h_{\rm s}^{1.4} + a_3 (\log D)^3 \\ & + a_4 e^{-h_{\rm obs}} h_{\rm s}^{3.7} + a_5 \left(\frac{1}{2}\right)^{h_{\rm obs}} (\log D)^2 + a_6 h_{\rm s}^{0.03} (\log D)^2 \\ & + a_7 e^{-h_{\rm obs}} e^{h_{\rm s}} \left(\frac{1}{2}\right)^{\log D} + a_8 h_{\rm obs}^{0.66} (\log D)^3 + a_9 h_{\rm obs}^{1.4} \\ & + a_{10} \left(\frac{1}{2}\right)^{h_{\rm obs}} (\log D)^6 + a_{11} h_{\rm s}^{1/6} e^{\log D} + a_{12} e^{3 \log D} \\ & + a_{13} h_{\rm obs}^{1.25} \left(\frac{1}{3}\right)^{\log D} + a_{14} (\log D)^9. \end{aligned} \quad (4)$$

Downloaded from https://academic.oup.com/mnras/article/519/1/26/6936422 by guest on 09 January 2025

Here, $a_0 = -0.544558$, $a_1 = -0.382289$, $a_2 = 0.0286502$, $a_3 = -0.119207$, $a_4 = -0.107372$, $a_5 = -0.484219$, $a_6 = -0.310468$, $a7 = 1.25005$, $a_8 = 0.0329962$, $a_9 = -0.0408976$, $a_{10} = 0.0071905$, $a_{11} = 0.0570251$, $a_{12} = -0.00296771$, $a_{13} = 0.0173055$, and $a_{14} = 0.000954598$.

2.1.5 *Horizontal irradiance*

The horizontal irradiance is not directly useful for astronomy but its importance as an environmental indicator, which gives the power per unit surface arriving from the artificial light scattered by the whole sky, suggests it should be included in this study.

The PSF of the indicator of the horizontal irradiance coming from the sky hemisphere has 13 terms, an RMSE of 0.0411, and an R^2 of 0.99957. Its analytical formula is

$$\begin{aligned}\log_{10} PSF_HorizontalIrradiance &= a_0 + a_1 h_{obs}^{0.43} + a_2 h_s^{1.95} \\ &+ a_3 2^{\log D} + a_4 h_{obs}^{-1.7} h_s^{1.9} + a_5 h_{obs}^{0.35} \log D + a_6 h_s^{0.41} (\log D)^3 \\ &+ a_7 h_{obs}^{-1.45} h_s^{1.8} \left(\frac{1}{2}\right)^{\log D} + a_8 h_{obs}^{0.18} e^{\log D} + a_9 e^{3 \log D} \\ &+ a_{10} h_s^{0.23} (\log D)^3 + a_{11} e^{-4 h_{obs}} + a_{12} (\log D)^4. \end{aligned} \quad (5)$$

Here, $a_0 = 2.56111$, $a_1 = -0.86252$, $a_2 = -0.00832378$, $a_3 = -1.8012$, $a_4 = -0.235985$, $a_5 = 0.716334$, $a_6 = 0.0861203$, $a_7 = 0.712949$, $a_8 = -0.0824399$, $a_9 = -0.000336386$, $a_{10} = -0.0686161$, $a_{11} = -0.170729$, and $a_{12} = 0.0558683$.

2.2. Calibration

In order to calibrate the output values obtained in the process described above, we took advantage of the calibration made for the NWA that used 20 000+ sky brightness measurements around the world. As the calibration of the NWA was made using a custom-made VIIRS data set of six months during 2014, we performed the calculation of the zenith radiance indicator matching the conditions of the NWA. In particular, we used PSFs with sources forced to be at sea level and observing sites at their altitude. These PSFs were applied to the exact same VIIRS data set used for the NWA. The computation of the indicator was made for a radius of 194 km around each observatory, as in the NWA. The ratio of the zenith radiance indicator over the zenith radiance value of the NWA should ideally give a constant value. In reality, this does not happen for several reasons, mainly because the general analytical PSF differs from the discrete PSFs (e.g. by up to 20 per cent in the case of an observatory at 2200 m and sources at sea level, but with only a 2.7 per cent RMS of the difference between the LOG10 of the discrete zenith PSF and the analytical PSF in the range of distances of the NWA). Moreover the pixel size of the NWA was 30 × 30 arcsec^2 in latitude–longitude projections while the new calculation was made with 15 × 15 arcsec^2 pixels, both for the VIIRS and digital elevation maps. We found significantly higher differences, sometimes off by more than a factor of 2, in the darkest sites, where the zenith radiance was approximately below 1×10^{-9} W m^{-2} sr^{-1}. After investigating several possible reasons, we found that the NWA data set (Falchi et al. 2016b) is imprecise at these very low artificial brightness levels. This arises from how the atlas was computed and assembled. In fact, for each of the 60 map tiles (30° × 30° wide in latitude and longitude) that cover the world, there were three tiles generated with the three different upward functions. An additional three tiles (for each of the 60 maps) were computed using as input the VIIRS data cut at a certain value of radiance. This was done because the output of the program was 16-bit integer fits with maximum at 32 768 and the program assigned the maximum value of the entire tile to the brightest pixel. Consequently, in the darkest sites of each tile, there is a quantization problem, with steps that are only as small as 1/32 768 of the brightest. At the end, for each of the 60 tiles maps, six tiles were merged. Notwithstanding this process, the very darkest places had quantization problems, generating steps. So, excluding for this work the nine darkest sites, below 1×10^{-9} W m^{-2} sr^{-1}, the final calibration factor to obtain radiance in W m^2 sr^{-1} resulted with a standard deviation of the mean of 1.7 per cent.

The calibration of the NWA was made using Sky Quality Meter (SQM) measurements acquired by other researchers and citizen scientists, assuming that commercial SQM magnitudes per arcsec^2 are equivalent to Johnson *V* magnitudes per arcsec^2 in a Vega +0.03 system. The calibration of the NWA was also checked with US National Park Service Johnson *V* band CCD measurements, resulting in very good agreement (see fig. 19 of Falchi et al. 2016a). For this work, we retrieved the *V* magnitudes from the NWA. If the Johnson *V* magnitude m_V is measured in the Vega scale, assigning to star Vega a *V* magnitude of +0.03 and using Vega's STIS003 spectrum, then, consistent with the *Gaia–Hipparcos* map scale, the linear physical quantity associated with m_V mag$_V$ arcsec^{-2} in the Vega +0.03 system will be the radiance (Masana et al. 2021):

$$L_V = 143.1685 \times 10^{-0.4\, m_V} \text{ W m}^{-2} \text{ sr}^{-1}. \quad (6)$$

3 RESULTS

The Johnson *V* radiance and irradiance indicators, latitude, longitude and altitude for all the studied sites are summarized in Table 1, divided into professional observatories (all those with 3 m or larger telescopes in action or planned for this decade), potential sites, other historic/control observatories (a small selection), observatories for amateur astronomers (a small selection where it is possible to rent telescopes) and control sites (for calibration purposes). In each category, the observatories are listed in order of increasing longitude.

The results of the zenith radiance and average radiance at 60° zenith distance (i.e. 30° above the horizon) are also shown in Figs 1 and 2. In this case, the values are expressed as a ratio to the chosen reference level of 22.0 mag$_V$ arcsec^{-2} for zenith and 21.8 mag$_V$ arcsec^{-2} for 30° above the horizon. The value of 22.0 is not chosen because it is the darkest possible natural level (in fact, darker skies are possible), but because it is commonly used as an arbitrary reference for natural pristine conditions (for some discussion, see, e.g. Falchi et al., 2016a; Green et al., 2022). It is worth mentioning that where natural sources of light are predominant, the variation of the natural airglow, the presence or not of the Milky Way (and what portions of it), the Zodiacal light, and the Gegenshein will change the radiance of the night sky significantly. The 21.8 reference level for 30° above the horizon derives from Falchi & Bará (2021), where the natural levels calculated with the *Gaia* map of the brightness of the natural sky (GAMBONS) were nearly 0.2 mag brighter at 30° compared to the zenith in the average over one year.

For two observatory sites, we presented two series of indicator values. Cerro Armazones, the future site for the ESO's Extremely Large Telescope, has one source of light very near. This turned out to be the lodge of the workers who are building the observatory. So, we also give the value of the indicators without this source of light, as when the observatory is operational we suppose that these lights will be always off. Mauna Kea is 'lit' by the dim red light

Downloaded from https://academic.oup.com/mnras/article/519/1/26/6936422 by guest on 09 January 2025

Table 3. Some statistical data of the analytical formulae for the PSFs of each indicator, as a result of the interpolation of multiple variables.

Indicator	Zenith radiance	Average all-sky radiance	Average radiance 30° above horizon	Average radiance 0° to 10° above the horizon	Horizontal irradiance
RMSE	0.04907	0.05386	0.05763	0.05933	0. 04110
R^2	0.99948	0.99886	0.99918	0.99878	0.99957
Number of terms	12	11	14	15	13

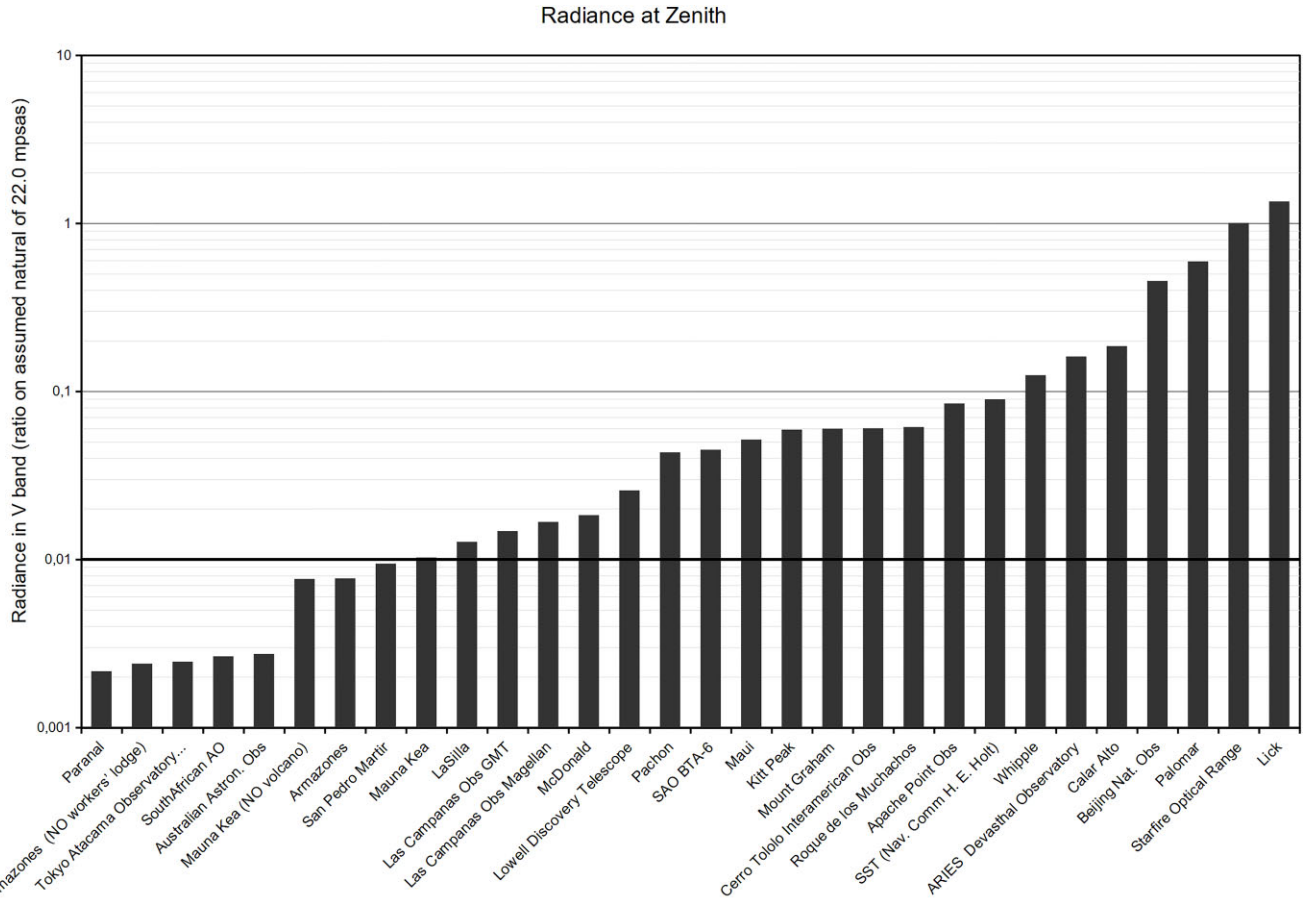

Figure 1. Calculated Johnson *V* radiance at zenith for all major observatories, as a ratio over an assumed background of 22.0 mag arcsec^{-2}. Only six (note that two observatories are reproduced twice; see the main text for the explanation) out of 28 observatories are below the 1 per cent increase of radiance over the assumed natural one (solid black line).

of the Kilauea volcano in the Hawaii Volcanoes National Park, at about 50 km from the observatory. We add a series of indicators excluding the contribution of the volcano. This is because its light is over-represented in satellite data, as the VIIRS detects near-infrared radiation, and a small fraction of the light emitted by the hot lava lies in the Johnson *V* band. Moreover, the light of the volcano is not artificial light. In 2021, the year of the VIIRS data set we used for our computations, there was also a volcanic eruption on La Palma, the island that hosts the Roque de Los Muchachos observatories. We checked if the light of the lava was present in the VIIRS data by comparing the data with the year 2020, finding no differences. The 2021 data are not affected by the eruption, probably because we used the median version of the VIIRS products.

One of the darkest sites (the third darkest amongst the professional observatories at zenith and sixth in the average radiance at 30°), where the University of Tokyo Atacama Observatory (TAO) is located, has a close source of pollution, at about 4 km, which contributes 38 per cent to its artificial zenith radiance and 8 per cent to its average radiance at 30°. This source of light pollution is the Atacama Large Millimeter Array (ALMA). So, the sky at the TAO is ironically threatened by light pollution coming from other astronomers. Without this source of light, TAO's sky would become the least polluted at zenith.

Our method allows us to disentangle the contribution of single sources, as identified by the pixel size of the satellite radiance data. As an example of this, we obtained the contribution of the lights along

Downloaded from https://academic.oup.com/mnras/article/519/1/26/6936422 by guest on 09 January 2025

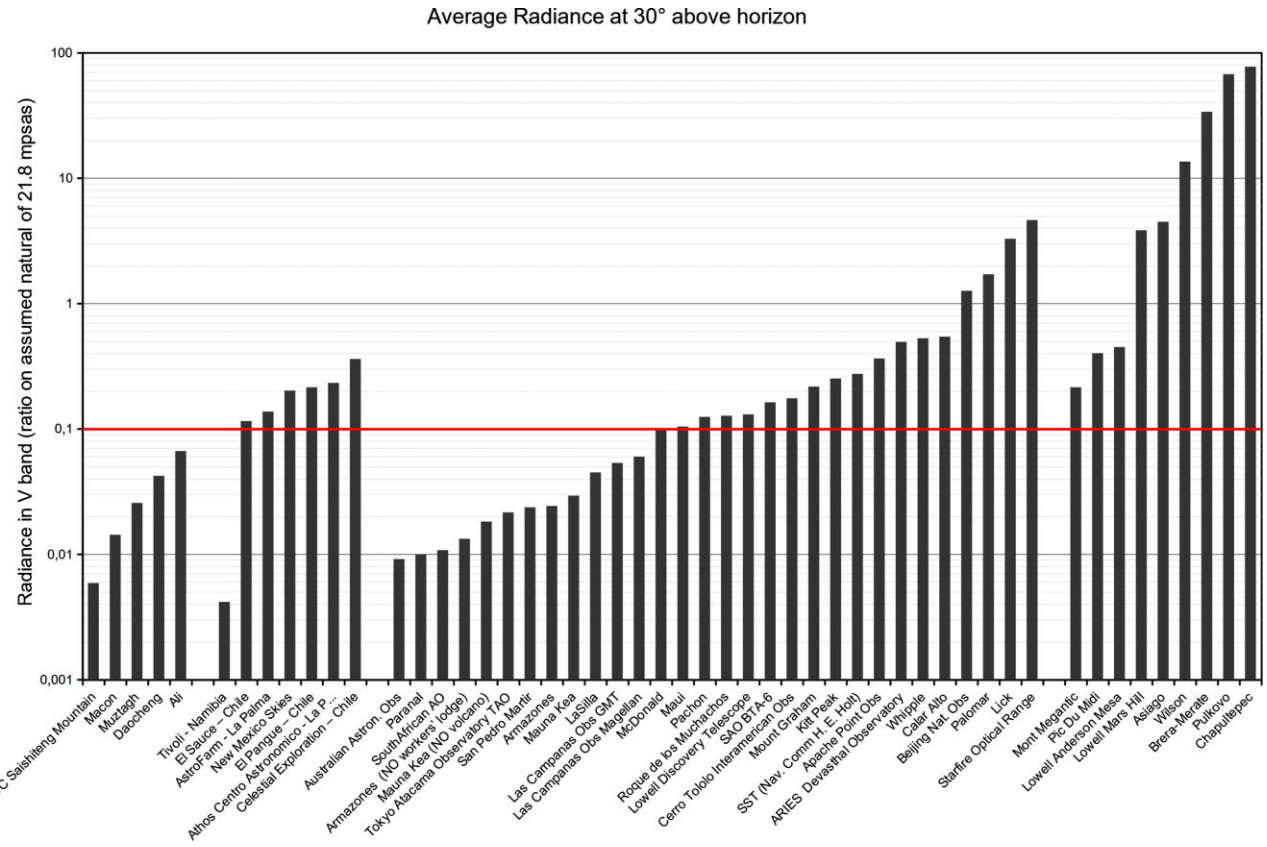

Figure 2. Calculated Johnson *V* average radiance at 30° above the horizon as a ratio over an assumed background of 21.8 mag arcsec^{-2}. The first group represents the potential sites, the second a selection of amateur sites, the third all the major observatories, and the fourth a selection of historic observatories sites. The red line indicates the 10 per cent increase above the assumed natural level.

the Ruta 5 highway near to the Giant Magellan Telescope (GMT) site at Las Campanas. We found that the lights of Ruta 5 alone, up to a distance of 40 km from the observatory, contribute to more than 50 per cent for both the artificial zenith radiance and the average radiance at 30°. The results are similar for the very near site of the twin 6.5-m Magellan Telescopes and also for ESO's La Silla observatory. Eliminating all the lights of Ruta 5, in the extra-urban part between La Serena and Vallenar, would cut the pollution even more.

4 DISCUSSION

Fig. 1 shows that only seven of the world's major observatories will stay under the 1 per cent increase over the 22.0 mag$_V$ arcsec^{-2} for zenith radiance, and two of these (i.e. San Pedro Martir and Mauna Kea) are close to this value. Note that also the Armazones site, with the lights of the workers' lodge on, is near this limit. The rest, three-quarters of the major astronomical observatories, surpass this value. The 1 per cent limit is the lowest pollution level used in the NWA, there represented in black in its maps. A night sky with this level of pollution can be considered pristine at high elevation above the horizon but it can still be heavily polluted at a few degrees above the horizon, as can be seen for the average radiance below 10° in Table 1, especially in the direction of specific sources of artificial light. Fig. 2 shows the situation of another indicator, the average radiance at 30° above the horizon, for all the studied sites, divided by their category. We display the 10 per cent artificial radiance limit with a red line in the figure. We found that almost two-thirds (18 out of 28) of major observatories have already surpassed this critical limit. It should be noted that we present here a value averaged along the whole azimuth, so the peak value is necessarily always higher (except in an ideally uniform pollution along all the azimuth angles). A comparison of the darkest sites in Figs 1 and 2 shows that having the darkest zenith does not necessarily result in having the best average sky at 30° above the horizon, and vice versa. All the major astronomical observatories in the continental USA have crossed the 10 per cent limit, while most Chilean observatories are still below it, even if some are relatively close. All three big Californian telescopes have surpassed the 10 per cent limit, by factors of 17 (Palomar), 33 (Lick) and, shockingly, 135 for the oldest of the three, the venerable Mount Wilson Observatory.

It is worth mentioning that the International Astronomical Union established a limit to the maximum tolerable artificial radiance of the night sky: the 'increase in sky brightness at 45° elevation due to artificial light scattered from clear sky should not exceed 10 per cent of the lowest natural level in any part of the spectrum between wavelengths 300 and 1000 nm' (Smith 1979). As our indicator gives the averaged value of the artificial radiance over all the azimuth angles and in a broad band of the visible spectrum, it is a more forgiving parameter compared with the peak value mentioned by the International Astronomical Union.

It is also worrying that some of the potential sites are not in as pristine conditions as we should expect for sites that are still to be developed and so will need several years or even decades to be exploited. So relatively small yearly increases may mean that these sites also cross the limit even before they become operational.

Our method (Bará et al. 2021) allows us to find the contribution to each indicator of the light coming from every single area of territory

Downloaded from https://academic.oup.com/mnras/article/519/1/26/6936422 by guest on 09 January 2025

surrounding the observatories, with the resolution of the radiance data used. The example, illustrated above, of the pollution coming from a single installation of lights along Ruta 5, contributing to about half the radiance from artificial light affecting the observatories of Las Campanas and La Silla, opens up the possibility of reversing locally the worldwide light pollution rising trend (Kyba et al. 2017; Sánchez de Miguel et al. 2021). In fact, this source alone, if eliminated, will cut by half the light pollution at the site of one of the next-generation giant telescopes.

None of our computations consider the artificial brightness caused by the ever-increasing number of satellites and space debris in low Earth orbit that have already raised the background brightness by about 10 per cent during some part of the astronomical night (Kocifaj et al., 2021). Adding this level of pollution would put all the night sky visible from the Earth's surface surpass the limit set by the International Astronomical Union.

5 CONCLUSIONS

We have presented the results of a comparison of all the major professional astronomical observatories, several potential sites, some historic observatories, and a few advanced amateur astronomical observatories. The comparison was made using five indicators of light pollution as computed with the Garstang–Cinzano propagation model applied to the VIIRS radiance data instrument onboard the *Suomi NPP* satellite. The results show that most astronomical major observatories are already significantly endangered by artificial light and some of them are very heavily polluted.

The outcomes emerging from this work are sending what might be the last call for a serious, collective, unambiguous, no-compromise action to lower light pollution now, whether it is generated from artificial light or from sunlight reflected by artificial objects in orbit. Failing to take action implies a progressive decline of our ability to explore our Universe. Astronomical observatories can be seen as the proverbial canary in a coal mine. If we are not able even to keep the canary alive, then we can forget being able to solve the problem of light pollution as a global environmental issue. In addition, all of the other negative consequences of light pollution will continue to rise, including biodiversity loss, the disruption of animal and human circadian rhythms, and negative health consequences for animals and humans (Sanders et al. 2021).

To maintain our ability to carry out top-grade astronomical research, it is necessary that the ALAN affecting observatories is reduced as soon as possible. Actions should also be taken in order to preserve potential sites for future observatories.

ACKNOWLEDGEMENTS

The authors declare that they have no competing interests. Part of this work was funded by Photonics4Life ED431B 2020/29 by Xunta de Galicia/Feder (FF), DIDULS/ULS, project PAAI2021 (MJ), NOIRLab, AURA, NSF (GD).

DATA AVAILABILITY

All data are available in the main text or, in case of the input data used for the computations (VIIRS radiance data and GMTED digital elevation model) in the references.

REFERENCES

Angione R. J., de Vaucouleurs G., 1986, PASP, 98, 1201
Bai C-H. et al., 2018, Res. Astron. Astrophys., 18, 107
Bará S., Falchi F., Lima R. C., Pawley M., 2021, Environmental Challenges, 5, 100212
Buton C. et al., 2013, A&A, 549, A8
Calabretta M. R., Greisen E. W., 2002, A&A, 395, 1077
Cinzano P., Elvidge C. D., 2004, MNRAS, 353, 1107
Cinzano P., Falchi F., Elvidge C. D., 2001a, MNRAS, 328, 689
Cinzano P., Falchi F., Elvidge C. D., 2001b, MNRAS, 323, 34
Cinzano P., Falchi F., Elvidge C. D., Baugh K. E, 2000, MNRAS, 318, 641
Danielson J. J., Gesch B. D. 2011, Global multi-resolution terrain elevation data 2010 (GMTED2010), US Geological Survey Open-File Report 2011–1073,
Elvidge C. D., Zhizhin M., Ghosh T., Hsu F-C., Taneja J., 2021, Remote Sensing, 13, 922
Falchi F. et al., 2016a, Sci. Adv., 2, e1600377
Falchi F. et al., 2016b, Supplement to: The New World Atlas of Artificial Night Sky Brightness. V. 1.1. GFZ Data Services
Falchi F., Bará S., 2021, Natural Sciences. 1, e10019
García-Gil A., Muñoz-Tuñón C., Varela A. M., 2010, PASP, 122, 1109
Garstang R. H.,1986, PASP, 98, 364
Garstang R. H.,1989, PASP, 101, 306
Green R. F., Luginbuhl C. B., Wainscoat R. J., Duriscoe D., 2022, A&AR, 30, 1
Gutierrez-Moreno A., Cortes G., Moreno H., 1982, PASP, 94, 722
Hayes D. S., Latham D. W., 1975, ApJ, 197, 593
Hogg D., Finkbeiner D. P., Schlegel D. J., Gunn J. E., 2001, AJ, 122, 2129
Kocifaj M., Kundracik F., Barentine J. C., Bará S., 2021, MNRAS, 504, L40
Kyba C. C. et al., 2017, Sci. Adv., 3, e1701528
Masana E., Carrasco J. M., Bará S., Ribas S. J., 2021, MNRAS, 501, 5443
Mohan V., Uddin W., Sagar R., Gupta S. K., 1999, Bulletin of the Astronomical Society of India, 27, 601
Patat F. et al., 2011, A&A, 527, A91
Sánchez de Miguel A., Bennie J., Rosenfeld E., Dzurjak S., Gaston K. J., 2021, Remote Sensing, 13, 3311
Sánchez S. F., Aceituno J., Thiele U., Pérez-Ramírez D., Alves J., 2007, PASP, 119, 1186
Sanders D., Frago E., Kehoe R., Patterson C., Gaston K. J., 2021, Nat. Ecol. Evol., 5, 74
Smith F. 1979, Transactions of the International Astronomical Union, 17, 218
Tapia M., Cruz-González I., Avila R., 2007, Rev. Mex. Astron. Astrofis., 28, 9

This paper has been typeset from a TEX/LATEX file prepared by the author.

Downloaded from https://academic.oup.com/mnras/article/519/1/26/6936422 by guest on 09 January 2025